Supporting Information for

Mechanistic interrogation on wound healing and scar removing by $Mo_{4/3}B_{2-x}$ nanoscaffold revealed regulated amino acid and purine metabolism

Dingkun Zhang[1,a], Man Zhu[2,a], Pei Xu[3,a], Xue Wen[4], Ge Liang[5], Wen Zheng[5], Yu Zeng[1], Tong Sun[6], Rong Fan[7], Yang Lu[7], Xueqin Tan[4], Meng Gong[1], Tingting Wang[8,*], Junjie Chen[4,*], Junwen Guan[1,6,*]

1. Department of Neurosurgery, Laboratory of Clinical Proteomics and Metabolomics, Institutes for Systems Genetics, Frontiers Science Center for Disease-related Molecular Network, National Clinical Research Center for Geriatrics, West China Hospital, Sichuan University, Chengdu 610041, P.R.China
2. Laboratory of Aging Research, School of Medicine, University of Electronic Science and Technology of China, Chengdu 610050, P.R.China
3. Department of Pathology, Deyang People's Hospital, Deyang 618000, P.R.China
4. Department of Plastic and Burn Surgery, West China Hospital, Sichuan University, Chengdu 610041, P.R.China
5. Metabolomics and Proteomics Technology Platform, West China Hospital, Sichuan University, Chengdu 610041, P.R.China
6. Department of Neurosurgery, West China Hospital, Sichuan University, Chengdu 610041, P.R.China
7. Department of Mechanical Engineering, City University of Hong Kong, Kowloon, Hong Kong SAR 999077, P.R.China; Chengdu Research Institute, City University of Hong Kong, Chengdu 610200, P.R.China
8. Department of Dermatology, West China Hospital, Sichuan University, Chengdu 610041, P.R.China

*Corresponding authors. E-mail: jwguan168@163.com, cjjemail@163.com, wangtingting817@126.com

a: These authors contributed equally to this work.

Chemicals and materials

Pristine $Mo_{4/3}B_{2-x}$ was obtained from Xinxi Technology Co., Ltd. (Foshan, China). The suspension of the above pristine $Mo_{4/3}B_{2-x}$ was freeze-dried to get the dry powder, stored in a sealed bottle and put in a dark place at the earliest for removing of unnecessary oxidation and decomposition of pristine $Mo_{4/3}B_{2-x}$. Institute of Cancer Research (ICR) mice were purchased from SPF Biotechnology Co., Ltd. (Beijing, China). All animal studies were carried out in accordance with the ethical regulations approved by the Ethics Committee of the Center for Animal Experiments of West China Hospital, Sichuan University, according to the 3 R principle of experimental animals (No. 20230301190). The hydrogel (Intrasite gel, No. 66597313) was obtained from Smith+Nephew Co. (England). Mouse fibroblast (L929) cells were obtained from the American Tissue Culture Collection (ATCC). Dulbecco's modified eagle medium (DMEM), cell culture plates were purchased from Corning Co. (NY, USA). Heat inactivated fetal bovine serum (FBS), penicillin-streptomycin solution, phosphate buffer saline (PBS), and trypsin were bought from Gibco (Thermo Fisher, USA). Double deionized water was used throughout the experiment. All chemical reagents in this experiment were analytical grade and utilized without further purification.

Characterization of $Mo_{4/3}B_{2-x}$ nanoscaffold

For fabrication of $Mo_{4/3}B_{2-x}$, 1 g pristine $Mo_{4/3}B_{2-x}$ was dispersed in 25 mL tetrabutylammonium hydroxide (TBAOH, 20% in water) under magnetic stirring for 24 h at room temperature. Then, TBAOH was eliminated through centrifugation (4500 rpm, 10 min, 22°C). The obtained precipitate was treated with a 0.22 μm filter and freeze-dried to obtain the dry powder, stored in a sealed bottle and put in a dark place at the earliest, which facilitated removing of unnecessary oxidation and decomposition. Such a treatment could guarantee the chemical stability of the obtained $Mo_{4/3}B_{2-x}$. The $Mo_{4/3}B_{2-x}$ nanoscaffold was prepared by mixing 5 mg $Mo_{4/3}B_{2-x}$ and 300 mg hydrogel for fine distribution of $Mo_{4/3}B_{2-x}$ in hydrogel. Such nanoscaffold could realize effective contact and absorption of $Mo_{4/3}B_{2-x}$ in wound and scar microenvironment with uniform and safe dosage.

The morphology of the $Mo_{4/3}B_{2-x}$ nanoscaffold was characterized by scanning electron microscopy (SEM, Sigma 500, Zeiss, Germany). Transmission electron microscopy (TEM, Tecnai G2 F20 S-TWIN, FEI, America) was applied under a 200 kV accelerating voltage. These micrographs were obtained by fully dispersing in water and drying in air on a copper grid. The X-ray diffraction (XRD) patterns of $Mo_{4/3}B_{2-x}$ nanoscaffold were obtained by using a Cu-Kα-irradiated Empyrean EMPYREAN diffractometer under the conditions of 40 kV voltage, 35 mA current, 14.79 s/d scanning speed, and 5° to 80° scanning angle. UV-Vis diffuse reflectance of $Mo_{4/3}B_{2-x}$ nanoscaffold was measured by UV-vis spectrophotometry (UV-1800, Shimadzu, Japan). Raman spectroscopy was obtained by SR-500i (Andor, England). X-ray photoelectron spectroscopy (XPS) was performed on ESCALAB 250Xi (ThermoFischer, USA), hv was 1486.6 eV. Water contact angle measurement was carried out on DSA100 (Kruss, Germany) with 300 × ∞ × 150 mm maximum volume, 0 to 180˚ range, +/- 0.01˚ resolution. Hemolytic test was performed on the blood of rabbit and the OD value was recorded on DS-11 (Denovix, USA).

Establishment of wound and scar model with $Mo_{4/3}B_{2-x}$ therapy

Mature male mice weighing between 22 and 25 g were applied to this study. The mice were raised in standard cages (6 mice per cage) at room temperature (22-24°C) with adequate ventilation, 12 h

light-dark cycle, constant temperature of 25 ± 0.5 °C, and approximately 50 ± 5% humidity. Commercial mice pellets and water were provided *ad libitum*. The animals were accustomed to the housing conditions for 7 days before starting the treatment. Subsequently, the mice were randomly divided into five groups of 7 mice each. After establishment of wound model (28 mice in four groups) or control (7 mice in the control group), later treatment was set as follows: control was given only normal diet and plain water; wound model (Wound) group was induced by creating a full-thickness excisional wound of approximately 1 cm^2 in size together with normal diet and plain water; wound model with $Mo_{4/3}B_{2-x}$ nanoscaffold therapy (Wound+$Mo_{4/3}B_{2-x}$) group was induced by creating a full-thickness excisional wound of approximately 1 cm^2 in size and therapy with 0.2 mg/g $Mo_{4/3}B_{2-x}$ nanoscaffold together with normal diet and plain water; scar model (Scar) group was induced by maintaining the full-thickness excisional wound of approximately 1 cm^2 in size with normal diet and plain water; scar model with $Mo_{4/3}B_{2-x}$ nanoscaffold therapy (Scar+$Mo_{4/3}B_{2-x}$) group was induced by maintaining the full-thickness excisional wound of approximately 1 cm^2 in size and therapy with 0.2 mg/g $Mo_{4/3}B_{2-x}$ nanoscaffold together with normal diet and plain water. Detailedly, the *in vivo* wound healing experiment was conducted following the established protocol[1]. The mice were anesthetized using pentobarbital sodium, and the dorsum was shaved and sterilized before creating a full-thickness excisional wound of approximately 1 cm^2 in size. According to the experimental grouping, one group of mice had their wounds covered with hydrogel, while the others had their wounds covered with a combination of hydrogel and 0.2 mg/g $Mo_{4/3}B_{2-x}$. An additional layer of sterile dressing was applied to cover the wounds to ensure sufficient contact with the material with the wounds. Post-surgery, the mice were allowed to recover in their respective cages. Wounds were re-dressed every other day, and the wound-healing process in each group of mice was systematically observed and documented. To quantify the progress of healing, the relative area of the wounds was determined by calculating the ratio between the area of the unhealed wound and the initially established wound area (approximately 1 cm^2). Re-epithelialization, a critical aspect of the healing process, was analyzed using Image J software (National Institutes of Health, USA). The calculation involved assessing the ratio between the distance covered by the re-epithelium and the distance between the wound margins (approximately 1 cm).

The *in vivo* scar removing was conducted at one month after wound modeling. After wounding, mice received hydrogel or hydrogel mixed with 0.2 mg/g $Mo_{4/3}B_{2-x}$ to cover the wounds. An additional layer of sterile dressing was applied to cover the wounds. Wounds were re-dressed every other day, and the therapy continues for one month post-modeling. Subsequently, the scars in mice from different groups were observed and documented. The scar tissues were then harvested and underwent histological and morphological studies to assess the severity of the scars.

Histological, morphological, and biochemical study on wound and scar

Histological staining was performed on paraffin sections. For morphology observation of the wound and scar, Hematoxylin-eosin (H&E) staining was carried out using an H&E staining kit (Solarbio, China). The heart, liver, spleen, lung, kidney, wound and scar from mice in these three groups were fixed in 10% buffered formalin for 48 h. Subsequently, the specimens were dehydrated and inserted in paraffin followed by sectioning to a thickness of 4 μm. These sections were then stained with H&E and observed under a GS3-U3-51S5M-C microscope (Point Grey, Canada). The concentration of Mo element in above tissues was determined by inductively coupled plasma optical emission spectrometer (ICP-OES). Additionally, Masson's trichrome staining, facilitated by a

Masson staining kit (Solarbio, China), was conducted to analyze collagen deposition within the wound and scar. Immunohistochemistry was performed on the paraffin sections using an SV Hypersensitivity Two-step Kit (Boster, China). The procedure involved dewaxing and hydrating the tissues, followed by antigen retrieval. Subsequently, the tissues were incubated overnight at 4 °C with primary antibodies targeting the following proteins: TNF-α (ab1793, Abcam, USA), IL-1β (ab315084, Abcam, USA), CD31 (ab124432, Abcam, USA), and α-SMA (ab5694, Abcam, USA). Following the primary antibody incubation, the tissues were exposed to the secondary antibody for an additional 0.5 hours. The visualization of targeted proteins was achieved by utilizing DAB-Substrate (Beyotime, China). Photomicrographs were captured using a microscope (ZEISS, Germany). The H-score method was employed to quantify the expression of the target proteins. The H-score was calculated using the formula: H-score = Σ (Pi × i), where i represents the intensity of staining, rated as 1 (weak), 2 (moderate), or 3 (strong). Pi denotes the percentage of stained cells corresponding to each intensity, ranging from 0% to 100%. The negative control was also set by using rabbit IgG (A7016, Beyotime, China) instead of primary antibodies, while the positive control was conducted on normal skin using the specific antibody. Scar elevation index (SEI) was measured for histomorphometry analysis as described previously from the H&E-stained tissue sections [2]. The SEI is a ratio of total wound area tissue height to the area of normal tissue. The height of normal tissue was determined based on the height of the adjacent unwounded dermis. An SEI of 1 indicates that the scar is of equal height to surrounding unwounded dermis; an SEI larger than 1 indicates a raised hypertrophic scar. SEI was measured examiners using Image-Pro Plus 6.0 software. Levels of vascular endothelial growth factor (VEGF) and transforming growth factor-β (TGF-β) in wound and scar tissues were analyzed using enzyme-linked immunosorbent assay (ELISA) kits (mlbio, China) according to the manufacturer's protocols. The intra-assay and inter-assay coefficients of variation were all less than 10%. Total protein concentration of each sample was analyzed by a BCA Protein Assay Kit (Beyotime, China) according to the manufactures' instructions. Samples were adjusted for total protein concentrations before ELISA was conducted to ensure that the amount of total protein in each group was equal. For superoxide production assays, total ROS production in wound and scar were tested by Reactive Oxygen Species Assay Kit (Beyotime, China). Additionally, superoxide dismutase (SOD) activity, glutathione peroxidase (GPx) activity, and malondialdehyde (MDA) accumulation in these tissues were analyzed by commercially available kits (Beyotime, China). The experimental steps for the aforementioned detection were strictly carried out in accordance with the instructions provided in the reagent kit. ROS level in wounds and scars from mice was analyzed according to the manufacturer's instructions. For dihydroethidine (DHE) staining, wounds and scars were embedded in Tissue-Tek OCT (Thermo Fisher). Then, the cryosections (10 μm) were incubated with the superoxide-sensitive dye DHE (10 μM in 0.01% DMSO) at 37°C for 30 min in a humidified dark cage. Then 4′,6-di-amidino-2-phenylindole (DAPI) was added to stain the nucleus. The fluorescence was observed by Laser Scanning Confocal Microscope (Leica, Germany) and analyzed by Leica Application Suite X (Leica, Germany). For western blotting, tissues were lysed with RIPA buffer to extract total proteins. Approximately 20 μg of proteins from each group were loaded onto a 10% SDS-PAGE gel for electrophoresis, followed by transfer onto a 0.45-μm polyvinyl difluoride (PVDF) membrane. After blocking with quick blocking buffer (Beyotime, China), the membrane was incubated overnight at 4 °C with primary antibodies against collagen I (ab270993, Abcam), collagen III (ab184993, Abcam), α-SMA (ab5694, Abcam), and GAPDH (ab8245, Abcam). Subsequently, the membrane was exposed to secondary antibodies for

0.5 h. Protein bands were visualized using an ECL Chemiluminescence Imager (Tanon, China) with an ECL plus kit (Beyotime, China). The relative expression of the target proteins was quantified using Image J software (National Institutes of Health, USA).

Metabolomics study

Wound and scar samples were also obtained from all experimental groups under general anesthesia. During this process, the wound and scar were collected and rinsed with PBS. For sample preparation, 20 mg of the wound and scar from each sample (n = 6) together with 6 steel balls and 200 μL precooled 80% CH_3OH were mixed three times for tissue homogenization (30 s each time). After vortexing at 1500 rpm for 10 s, the above suspension was quenched with 800 μL precooled 80% CH_3OH at -80°C for 30 min. Then, this mixture was subjected to ultrasonication (30 min) in an ice bath and centrifugation (13000 rpm, 10 min, 4°C). After that, 1 mL of supernatant was collected and dried at 30°C for 3 h. Before LC-MS/MS detection, the above dried aqueous-soluble samples were re-dissolved in 500 μL of HILIC solution (10 mM ammonium acetate in 30% water/70% CH_3CN + 0.2% acetic acid containing ^{13}C2-L-tyrosine and ^{13}C1-L-lactate) followed by sonicating 3 min and vortexing at 1500 rpm for 30 min. Finally, sonicating 3 min and centrifugation (13300 rpm, 4˚C, 10 min). The 100 μL supernatant obtained was kept aside for later analysis. The quality control (QC) sample was a mixture containing 20 μL of each sample. A LC-MS/MS system, AB Sciex triple quadrupole 6500 mass spectrometer mass spectrometer coupled with Nexera LC-30A UPLC system (AB Sciex, Framingham, MA), was used for analysis by multiple reaction monitoring (MRM) mode. The 228 metabolites (99 in positive mode and 128 in negative mode) chosen for such analysis represented major metabolic pathways. UPLC conditions contain a flow rate of 300 μl/min with a mobile phase of (A) 10% acetonitrile in water (including 10 mM ammonium acetate and 0.2% acetic acid) and (B) 90% acetonitrile in water (containing 10 mM ammonium acetate and 0.2% acetic acid). The ACQUITY UPLC BEH Amide column (2.1 mm × 100 mm, 1.7 μm, Waters, UK) was heated to 40˚C. Injection volume was 5 μL (positive modes) or 10 μL (negative modes). The MS was composed of a heating electrospray ionization (H-ESI) source. For positive mode, the interface capillary was kept at 500˚C with a ion source gas flow (Gas1) of 50 psi and ion source gas flow (Gas2) of 40 psi. The ionspray voltage was 5.5 kV. For negative mode, the interface capillary was kept at 550˚C with a ion source gas flow (Gas1) of 50 psi and ion source gas flow (Gas2) of 40 psi. The spray voltage was -4.5 kV. All the samples were injected at random.

Statistical analysis

The raw data was imported into SCIEX OS (v2.0) for pretreatment. The pretreated data, including sample information, metabolite identity, and peak intensities were further processed in R (v3.5.1). During such process, the interpolation of missing value was accomplished by k-nearest neighbor (KNN) algorithm [3], and QC-based robust locally estimated scatterplot smoothing (LOESS) signal correction (QC-RLSC) was normalized [4]. Next, principal component analysis (PCA), partial least squares discrimination analysis (PLS-DA) and orthogonal partial least squares discriminant analysis (OPLS-DA) were applied to discriminate above five groups. The p values ($p < 0.05$) in the t tests and variable importance of the obtained data in the projection (VIP) value (VIP > 1) in the OPLS-DA model were set for all metabolites. The metabolic network and pathway analysis of the metabolome were performed according to MetaboAnalyst (v5.0).

Establishment of wound in diabetes model with $Mo_{4/3}B_{2-x}$ therapy

We followed the previously described method to induce diabetes in mice models [1]. Briefly, mice were intraperitoneally injected with streptozocin (STZ) (S0130, Sigma-Aldrich, USA) at a dose of 100 mg/kg, dissolved in 0.01 M citrate buffer (pH 4.5). These injections were administered twice a week, while the mice were in a fasting state. Blood glucose levels were monitored every 2 days post-STZ injection using an Accu-Check Active glucometer (Roche, Lyon, France). Diabetes was defined by the blood glucose level reached or exceeded 250 mg/dL. After the induction of diabetes, full-thickness excisional wounds were meticulously created on the dorsal skin of diabetes mice, under anesthesia state. According to the experimental grouping, one group of mice had their wounds covered with hydrogel, while the others had their wounds covered with a combination of hydrogel and 0.2 mg/g $Mo_{4/3}B_{2-x}$. An additional layer of sterile dressing was applied to cover the wounds to ensure sufficient contact with the material with the wounds. Later experiment was the same as that in previous *in vivo* wound healing experiment.

***In vitro* ROS-removing activity of $Mo_{4/3}B_{2-x}$ nanoscaffold**

Mouse fibroblast (L929) cells were cultured in DMEM medium containing 10% FBS and 1% penicillin-streptomycin solution, and incubated in an atmosphere of 5% CO_2 at 37˚C in a humidified incubator. The medium was changed every two days to maintain cell viability, whereas all other conditions remained the same. The cells were subcultured with 0.25% trypsin. L929 cells with exponential growth were utilized in all the experiments. Before exposure to $Mo_{4/3}B_{2-x}$ nanoscaffold, L929 cells were first rinsed with PBS, then 1 mL 0.25% trypsin was added and resuspended in a fresh medium of 5×10^5 cells/ml. Then, 2 mL L929 cells were finely dispersed and divided into six parts on an average and inoculated into each hole of the 6-hole plates. Adherent L929 cells were then exposed to 2 mM H_2O_2 or 1 mg/mL of $Mo_{4/3}B_{2-x}$ nanoscaffold + 2 mM H_2O_2 with gently shaken to obtain sufficient dispersion. The samples were then incubated in a humidified incubator for another 30 min. Each experiment was repeated five times. Cell apoptosis was measured by Annexin V and propidium iodide (PI) dual staining (4A Biotech Co., Ltd, China). Briefly, L929 cells were incubated with 5 μL Annexin V-FITC for 5 min at room temperature in the dark, and then mixed with 10 μL PI. The apoptosis rate was determined by flow cytometry analysis (Annexin V/FITC, Ex/Em: 488nm/525 nm; PI, Ex/Em: 561nm/575 nm). CCK-8 kit (Solarbio, Beijing, China) was used to examine the cell proliferation by absorbance assay. 1×10^3 cells were seeded into each pore of 96 pore plates. 10 μL of CCK-8 solution was added to each pore with incubation for 1 hour in the dark at 37˚C. The cell viability was detected by absorbance at 450 nm on Synergy MX microplate reader (BioTek, America). The level of ATP was determined by ATP assay kit (Beyotime Co., Beijing, China). For superoxide production assays, total ROS production in cells was tested by Reactive Oxygen Species Assay Kit (Beyotime, China). Additionally, SOD, GPx, and MDA accumulation in cells were analyzed by commercially available kits (Beyotime, China). For the assessment of intracellular oxidative stress, L929 cells were incubated with DCFH-DA (10 μM, S0033S, Beyotime Co., Beijing, China) at 37˚C for 30 min. Fluorescence intensity was detected and recorded by a flow cytometer (Ex/Em: 488nm/525 nm; Beckman Coulter cytoFLEX, USA). For measurement of mitochondrial superoxide production, the L929 cells were incubated with MitoSOX Red (2.5 μM, Invitrogen, Fisher, USA) at 37 ˚C for 30 min, rinsed with PBS and resuspended in 200 μL PBS for flow cytometry analysis (Ex/Em: 510nm/580 nm; Beckman Coulter cytoFLEX, USA). For glycolysis stress assay, XF glycolysis stress test kit (Agilent, CA, USA) was used to test

the glycolytic function of L929 cells using a Seahorse Extracellular Flux Analyzer (Seahorse Bioscience, USA). L929 cells were seeded in XF24 cell culture microplates (4×10^4 cells/well) and incubated at 37˚C overnight. The medium was replaced with Mito Stress assay medium containing 5 mM glutamine (pH 7.4). Then, above microplates were incubated at 37˚C in a non-CO_2 incubator for 1 h. Three kinds of solutions were injected into corresponding holes: A port: 10 mM glucose; B port: 1 μM oligomycin; C port: 50 mM 2-deoxyglucose. The extracellular acidification rate (ECAR) was tested at three time points between injection of each compound. For mitochondrial stress assay, XF cell mito stress test kit (Agilent, CA, USA) was applied to test mitochondrial function with the same equipment. L929 cells were seeded in XF24 cell culture microplates (4×10^4 cells/well) and incubated at 37˚C overnight. The medium was replaced with Mito Stress assay medium containing 25 mM glucose, 2 mM pyruvate and 2 mM glutamine (pH 7.4). Then, above microplates were incubated at 37˚C in a non-CO_2 incubator for 1 h. Three kinds of solutions were injected into corresponding holes: A port: 1 μM oligomycin; B port: 1 μM carbonyl cyanide-4 (trifluoromethoxy) phenylhydrazone; C port: 0.5 μM rotenone/antimycin A. Mitochondrial oxygen consumption rate (OCR) values were tested at three time points between injection of each compound. The obtained data were recorded and calculated with Seahorse XF-24 analyzer software (Seahorse Bioscience, USA).

Reference

1. Wen, X.; Zhu, M.; Li, Z.; Li, T.; Xu, X., Dual effects of bisphenol A on wound healing, involvement of estrogen receptor β. *Ecotoxicol Environ Saf* 2022, 231, 113207.
2. Cheng, L.; Sun, X.; Zhao, X.; Wang, L.; Yu, J.; Pan, G.; Li, B.; Yang, H.; Zhang, Y.; Cui, W., Surface biofunctional drug-loaded electrospun fibrous scaffolds for comprehensive repairing hypertrophic scars. *Biomaterials* 2016, 83, 169-81.
3. Lee, J. Y.; Styczynski, M. P., NS-kNN: a modified k-nearest neighbors approach for imputing metabolomics data. *Metabolomics* 2018, 14.
4. Shisheng; Wang; Xiaolei; Chen; Dan; Wen; Zheng; Liqiang; Hao; Yang, MetaboGroupS: A Group Entropy-based Web Platform for Evaluating Normalization Methods in Blood Metabolomics Data from Maintenance Hemodialysis Patients. *Analytical chemistry* 2018.

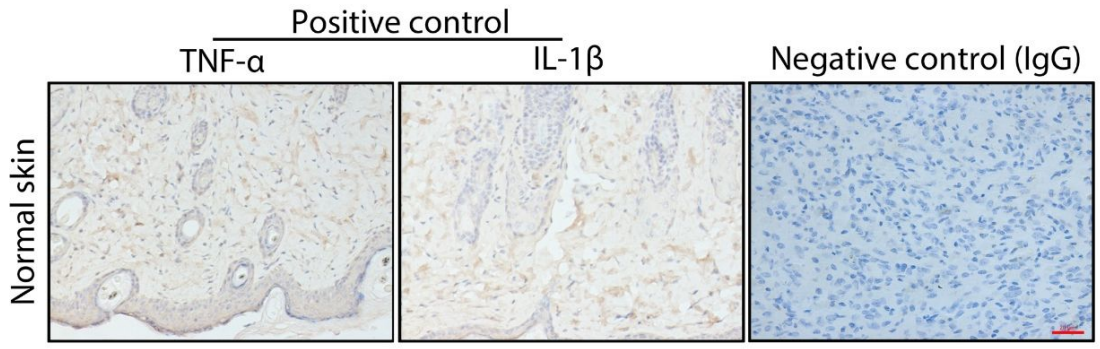

Fig. S1 Positive and negative control of immunohistochemical staining using normal skin. The positive control of immunohistochemical staining showed yellow-brown particles within tissues whereas the negative control showed no positive staining. Scale bar: 20 μm.

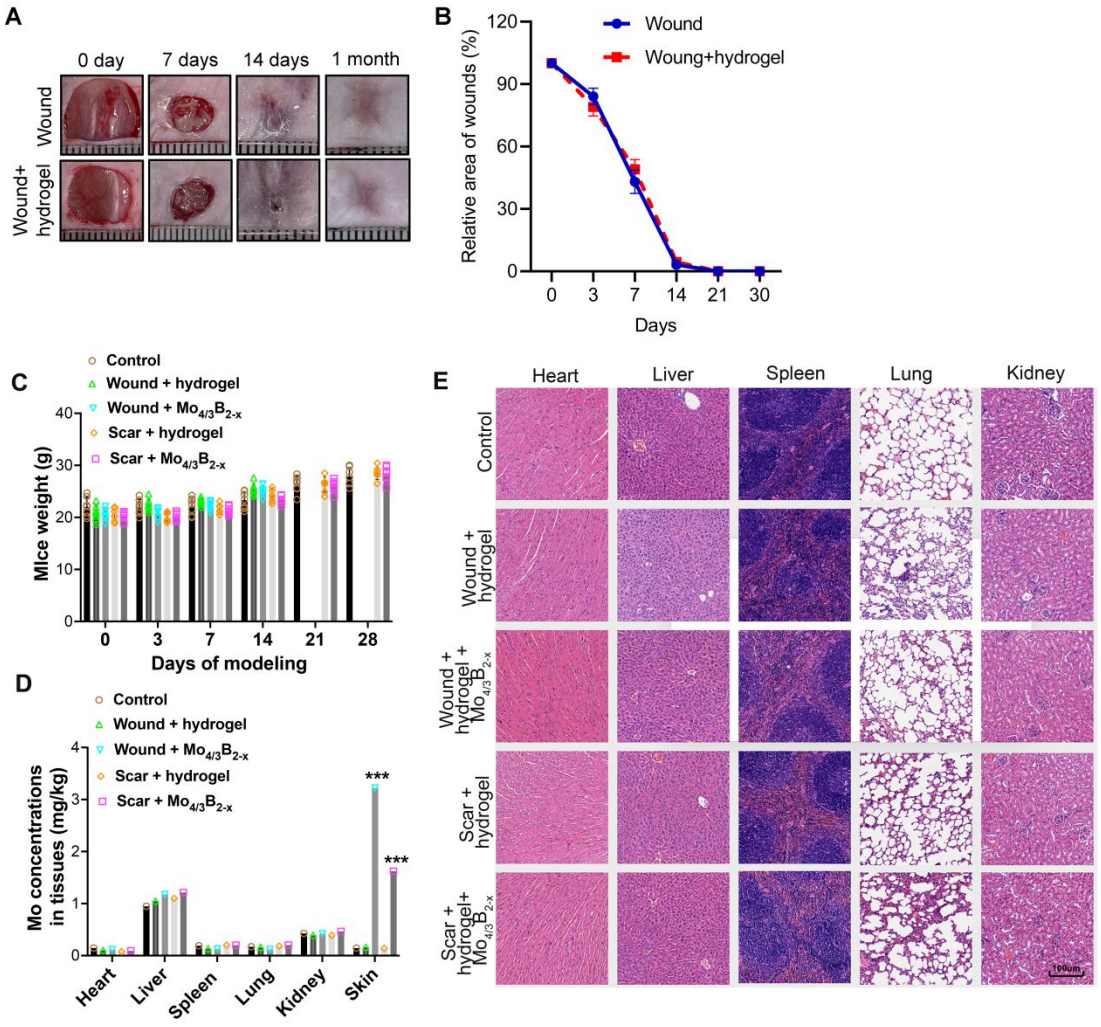

Fig. S2 Toxicity assessment of the $Mo_{4/3}B_{2-x}$ applying on wound or skin. (a) Photographs indicating the status of wound healing with hydrogel in mice from different groups. (b) Quantitative analysis on wound healing with hydrogel. (c) Weight change in mice from different groups. (d) $Mo_{4/3}B_{2-x}$ level in heart, liver, spleen, lung, kidney, and skin tissues of mice from different groups. (e) Histological staining of heart, liver, spleen, lung, and kidney tissues of mice from different groups. Scale bar: 100 μm. Seven mice in each group. Data were shown as mean ± SD. *: $p < 0.05$, **: $p < 0.01$, ***: $p < 0.001$.

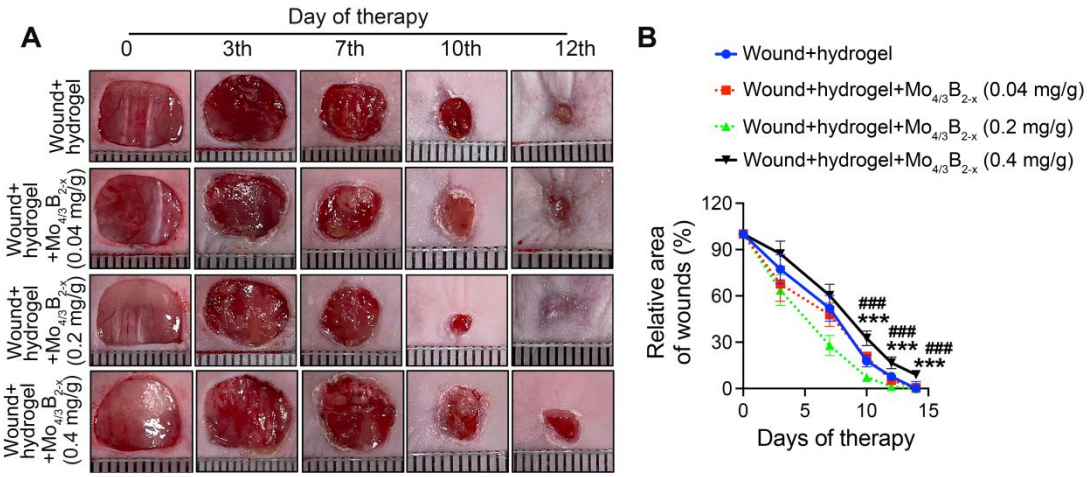

Fig. S3 Effects of different concentrations of $Mo_{4/3}B_{2-x}$ on wound healing. (a) Photographs indicating the status of wound healing in mice treated with $Mo_{4/3}B_{2-x}$ at the dosages of 0.04 mg/g, 0.2 mg/g, and 0.4 mg/g. (b) Quantitative analysis revealed that 0.2 mg/g of $Mo_{4/3}B_{2-x}$ promoted healing significantly whereas 0.4 mg/g of $Mo_{4/3}B_{2-x}$ delayed wound healing markedly. Seven mice in each group. Data were shown as mean ± SD. *: Difference between Wound group and Wound+$Mo_{4/3}B_{2-x}$ (0.2/mg/g) group; $^{\#}$: Difference between Wound group and Wound+$Mo_{4/3}B_{2-x}$ (0.4/mg/g) group. $^{*/\#}$: $p < 0.05$, $^{**/\#\#}$: $p < 0.01$, $^{***/\#\#\#}$: $p < 0.001$.

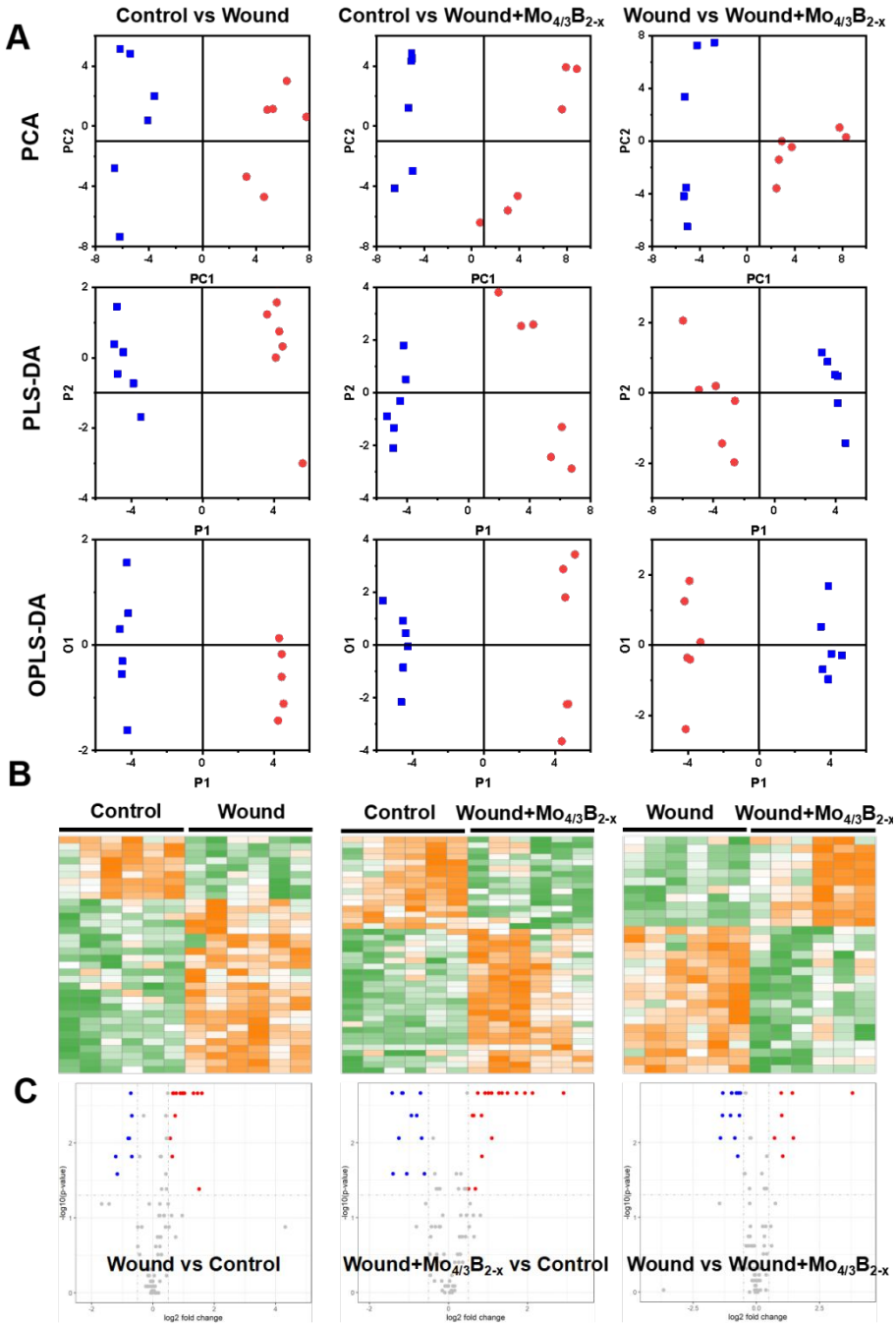

Fig. S4 Metabolomics study on $Mo_{4/3}B_{2-x}$ nanoscarffold-induced wound healing. (a) PCA score plots of PC1 vs PC2, PLS-DA score plots of p1 vs p2, OPLS-DA score plots of p1 vs o1. In Control vs Wound group, blue dots: control, red dots: Wound group; In Control vs Wound+$Mo_{4/3}B_{2-x}$ group, blue dots: control, red dots: Wound+$Mo_{4/3}B_{2-x}$ group; In Wound group vs Wound+$Mo_{4/3}B_{2-x}$ group, blue dots: Wound group, red dots: Wound+$Mo_{4/3}B_{2-x}$ group. Permutation test: $pR^2 = 0.01$, $pQ^2 = 0.01$. (b) The extracted heatmaps of differential metabolites. The color scale illustrates the relative abundances across the samples. Correspondingly, orange indicates significantly upregulated metabolites, while green indicates metabolites that were significantly downregulated. (c) Volcano plots of all detected and quantified metabolites.

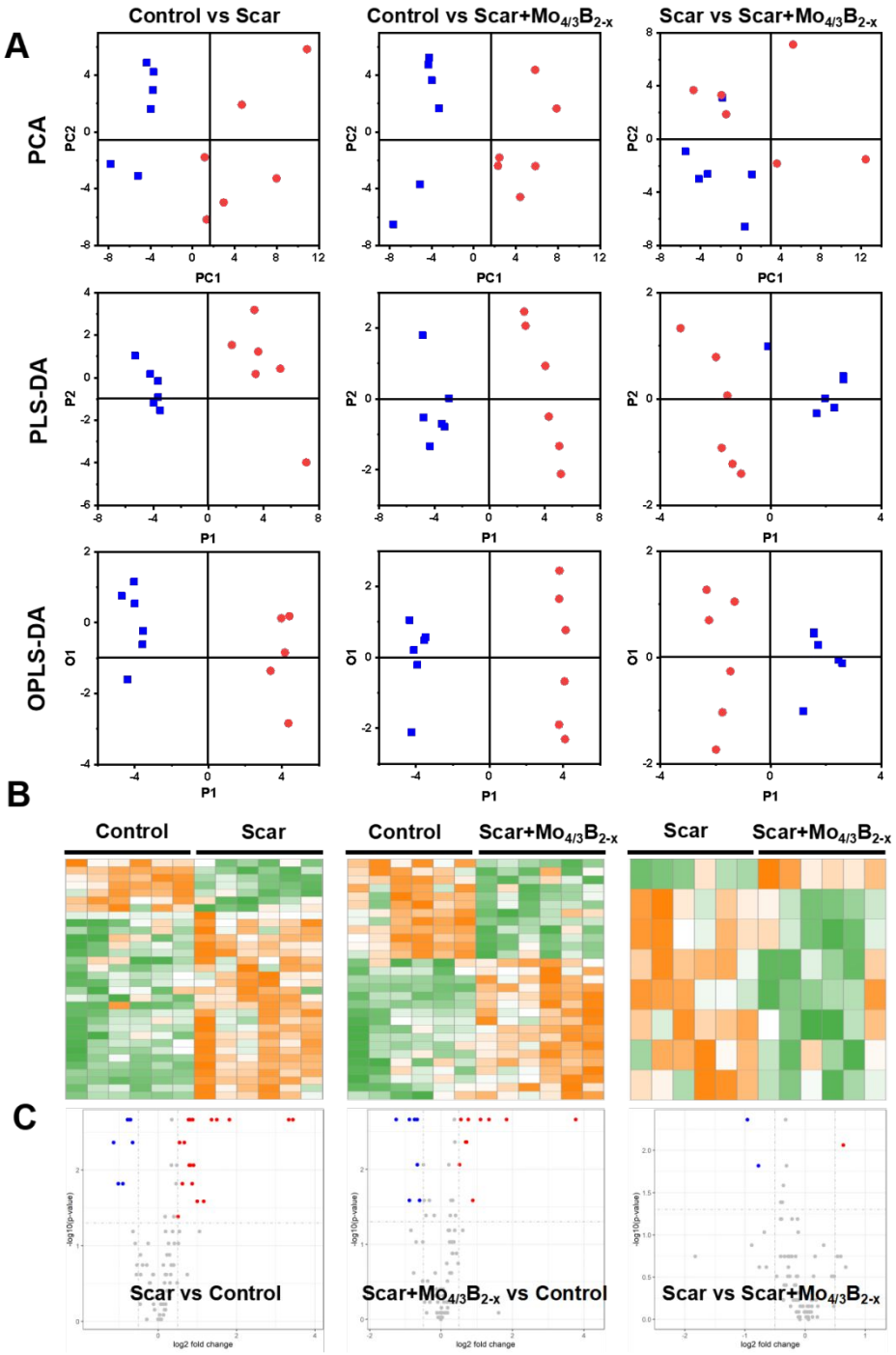

Fig. S5 Metabolomics study on $Mo_{4/3}B_{2-x}$ nanoscarffold-induced scar removing. (a) PCA score plots of PC1 vs PC2, PLS-DA score plots of p1 vs p2, OPLS-DA score plots of p1 vs o1. In Control vs Scar group, blue dots: control, red dots: Scar group; In Control vs Scar+$Mo_{4/3}B_{2-x}$ group, blue dots: control, red dots: Scar+$Mo_{4/3}B_{2-x}$ group; In Scar group vs Scar+$Mo_{4/3}B_{2-x}$ group, blue dots: Scar group, red dots: Scar+$Mo_{4/3}B_{2-x}$ group. Permutation test: $pR^2 = 0.01$, $pQ^2 = 0.01$. (b) The extracted heatmaps of differential metabolites. The color scale illustrates the relative abundances across the samples. Correspondingly, orange indicates significantly upregulated metabolites, while green indicates metabolites that were significantly downregulated. (c) Volcano plots of all detected and quantified metabolites.

Table S1 Experimental and characterization data of $Mo_{4/3}B_{2-x}$ nanosheets

	$Mo_{4/3}B_{2-x}$
Dimension	2
Morphology	nanosheets
Element mapping	fine distribution of Mo and B elements
EDX analysis	coexistence of Mo and B elements
XRD peaks	34.00° and 39.79°
UV-vis curve	strong absorption in a wide range
Raman spectrum	Typical peaks at 332.7, 412.5, 632.9, 747.5 and 200.2 cm^{-1}
XPS survey spectra	presence of Mo and B elements
XPS spectra (Mo 3d)	Mo^{4+} (234.5 and 229.0 eV), Mo^{5+} (235.6 and 232.3 eV), Mo^{6+} (236.5 and 233.4 eV), and Mo-B-Tz (230.9 and 227.8 eV)
Water contact angle measurement	high hydrophilicity (50.6°-53.6°)
Hemolytic test	negligible hemolysis of red blood cell (2.4%)

Table S2 Experimental and characterization data of $Mo_{4/3}B_{2-x}$ nanoscaffold

	$Mo_{4/3}B_{2-x}$
Morphology	porous structure
Element mapping	fine distribution of Mo and B elements
EDX analysis	presence of Mo, B and C elements
Element content	Mo (3.14 wt%), B (11.87 wt%) and C (84.99 wt%)
Application	$Mo_{4/3}B_{2-x}$ nanoscaffold and dressing
Advantage	stable and long-term therapeutic process through fixing and preserving $Mo_{4/3}B_{2-x}$ nanoscaffold

Table S3 Differential metabolic pathways and metabolites in wound model

Metabolic pathway	Metabolites
Amino acid metabolism	Serine, Threonine, Leucine, Histamine, Glutamine, Proline, 4-Hydroxyproline
Purine metabolism	Urate, Adenine, Adenosine, Creatine

Table S4 Differential metabolic pathways and metabolites in scar model

Metabolic pathway	Metabolites
Amino acid metabolism	Serine, Threonine, Histamine, Proline
Purine metabolism	Xanthosine, Adenine, Adenosine, Creatine, Guanosine
Glycolysis	Glucose-6-phosphate
TCA cycle	Succinate